Transmission resonances and zeros in quantum waveguide systems with attached resonators

Zhi-an Shao, Wolfgang Porod, and Craig S. Lent
Department of Electrical Engineering, University of Notre Dame, Notre Dame, Indiana 46556
(Received 17 May 1993; revised manuscript received 20 September 1993)

Transmission phenomena in quantum waveguide structures are studied by examining the transmission amplitude in the complex-energy plane. We find that, similar to double-barrier resonant tunneling, there are transmission poles in the complex-energy plane for quantum waveguide structures which contain quasibound states in attached t-stub resonators. In contrast to double-barrier resonant tunneling, however, we find that the quantum-wire networks also possess transmission zeros (antiresonances), which always occur on the real-energy axis. The existence of transmission zeros is a characteristic feature of a quantum waveguide system with attached resonators, but is absent for double-barrier resonant tunneling, which contains the resonant cavity as part of the transmission channel. We demonstrate that each quasibound state of the resonantly coupled quantum waveguide system leads to a zero-pole pair of the transmission amplitude in the complex-energy plane. The previously noted resonance-antiresonance behavior of the transmission probability, which leads to its sharp variation as a function of energy, can be understood in terms of these zero-pole pairs.

I. INTRODUCTION

Electronic transport in ultrasmall semiconductor structures reveals the quantum-mechanical wave nature of the charge carriers. As shown in papers by Landauer and Büttiker,[1,2] electronic conduction in this so-called mesoscopic regime[3] can be viewed as a transmission problem, and the conductance is related to the transmission coefficient by the quantum unit of conduction e^2/h. Much work has been inspired by analogous wave phenomena in optics and the possibility of utilizing resonant transmission behavior for electronic device applications.[4] Fabry-Pérot-like transmission resonances in semiconductor superlattice structures have been studied since the seminal work of Esaki and Tsu.[5] The phenomenon of double-barrier resonant tunneling (DBRT) is well understood, and practical devices based on this concept, even operating at room temperature, have been developed.[6] Recent work has focused on transmission in electronic waveguides and related quantum interference devices, and it has been noted that resonance phenomena in these structures give rise to rich features in the transmission coefficients.[7,8]

In this paper we investigate resonance phenomena for transmission in quantum waveguide structures by studying the transmission amplitude in the complex-energy plane. In analogy to double-barrier resonant tunneling, we find that transmission resonances are related to the existence of quasibound states. There is one major difference, however, as pointed out by us in a recent paper.[9] DBRT gives rise to the well-known Lorentzian-shaped Breit-Wigner transmission resonances, which correspond to poles in the complex-energy plane. The transmission probability for resonantly coupled waveguides, on the other hand, exhibits resonance-antiresonance features, which correspond to zero-pole pairs in the complex transmission amplitude. We will demonstrate that these antiresonances, in fact, are zeros and that their existence is a consequence of unitarity.

Resonance-antiresonance features including sharp transmission minima have been seen in recent numerical work on conduction in quantum waveguide structures and for transmission through an oscillating barrier.[10] A much studied system consists of a main transmission channel with an attached t-stub resonator.[11–17] Sharp drops to a minimum are observed in the transmission coefficient (we will show that those, in fact, are zeros), and forbidden bands are formed for multiple-stub systems.[18–20] Using a scattering-matrix approach,[21] Price[22] shed light on the relationship between the transmission coefficient and the quasibound states in the resonant t stubs. Another example of a resonantly coupled waveguide consists of a channel which is connected to a circular cavity.[23] In this system, the quasibound states in the cavity are excited at resonant energies by the electron flow in the channel, giving rise to sharp structure in the transmission probability. Narrow current dips have been investigated for resonant-tunneling structures with quantum dots.[24] Impurities in a transmission waveguide also give rise to conduction in the presence of quasibound states, and resonance effects have been observed in several studies.[25–31] Geometric effects in conduction channels may also result in bound states,[32] and the transmission coefficient has been studied for bends,[33,34] corners,[35,36] crosses,[37–40] etc. The sharp drops of the transmission probability are also found in loop structures.[41–44] Similar resonant behavior has also been reported for transmission in systems where several electronic subbands are available. Such studies include electronic Γ-X conduction-band minima[45–47] and heavy-hole–light-hole[48,49] interference effects for resonant tunneling in double-barrier heterostructures. Common to all of the above examples is that resonance features are observed when more than one scattering channel is available.[50] When continuum states interact with localized states, two scattering channels are available, one belong-

ing to a continuum and the other to a bound state. These so-called Fano resonances[51] have first been studied for the interaction between light and electrons from atoms and molecules.

Experimental evidence is available in support of coherent transport, required for the large body of theoretical work cited above. In two-dimensional electronic systems, elastic mean free paths of virtually macroscopic dimensions have been reported and applied to ballistic-electron optics.[52] In a related study, ballistic-electron propagation was observed over a distance of 210 μm in a four-terminal square device.[53] In confined geometries, interference phenomena have been reported in a periodically corrugated ballistic channel of 3 μm length, leading to the formation of bands and gaps.[54] Modulation of the conductance in T-shaped electron waveguide structures has been observed;[55] however, it was not unambiguously established in that paper that these oscillations were due to quantum interference effects. In a more recent paper, evidence was presented for quantum interference giving rise to conductance oscillations in a 1.2-μm-long quantum wire with a stub structure.[56] Very recently, a combined experimental and theoretical analysis supported the existence of waveguide effects in quantum wires with double-bend discontinuities.[57–59] Coherent transport over distances of 2–4 μm has been observed in single and multiple wires and rings.[60,61]

The prototypical system studied in this paper consists of a resonator which is coupled to an incoming and an outgoing lead. An incident wave impinges upon the resonator structure under study, and transmitted and reflected waves emerge. The classes of systems investigated here are comprised of double-barrier resonant-tunneling and quantum-wire networks with attached t stubs. The quasi-one-dimensional problem of DBRT can be thought of as transmission in a quantum wire which contains two barriers, as schematically shown in the inset of Fig. 1(a); the potential barriers on the channel are represented by the shaded boxes. The insets of figures throughout the paper show a variety of strongly and weakly coupled t stubs which will be investigated. Utilizing both wave-function matching and finite-element methods,[62] the time-independent Schrödinger equation is solved to obtain the transmission amplitude in the complex-energy plane for both double-barrier resonant tunneling and the quantum waveguide structures. We assume that an incoming wave with energy E, incident upon the system from the left, results in a reflected and transmitted wave. The wave functions in the asymptotic regions on the left and right are given by,

$$\psi_L(x,k)=\exp(ikx)+r(k)\exp(-ikx)\ , \tag{1a}$$

$$\psi_R(x,k)=t(k)\exp(ikx)\ . \tag{1b}$$

Here $k=\sqrt{2m^*E}/\hbar$ is the complex wave-vector variable ($m^*=0.067m_0$), and $r(k)$ and $t(k)$ denote the reflection and the transmission amplitudes, respectively. Our analysis concentrates on the analytic behavior of these functions, in particular on the zeros and/or poles which represent the quasibound states in the resonators.

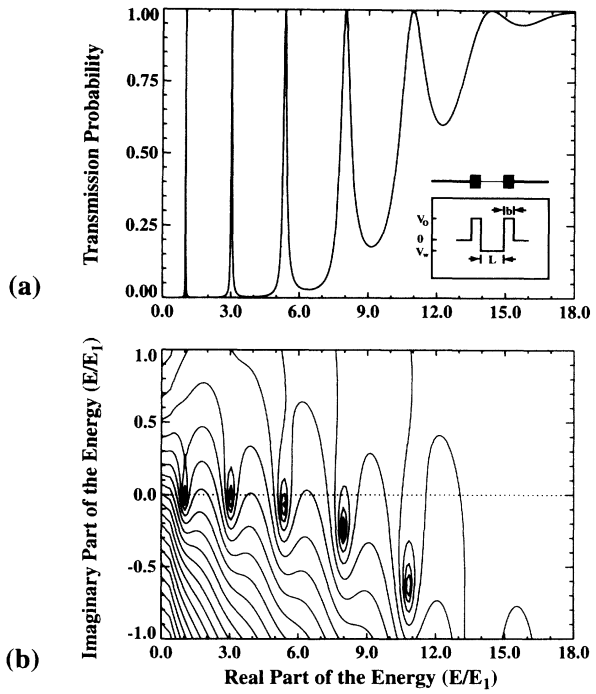

FIG. 1. Transmission coefficient for a double-barrier resonant-tunneling structure which is schematically depicted in the inset ($V_0=0.2$ eV, $V_W=-0.1$ eV, $L=30$ nm, and $b=5$ nm; energy of the first transmission peak $E_1=28.2$ meV); (a) shows the transmission probability on the real-energy axis and (b) shows a contour plot of the absolute value of the transmission amplitude in the complex-energy plane.

The transmission amplitude $t(k)$, or $t(E)$, for an incoming wave with wave number k, or energy E, is then obtained from the outgoing wave function ψ_R by

$$t(k)=\psi_R(x_0,k)e^{-ikx_0}\ , \tag{2}$$

with x_0 fixed. The transmission amplitude may also be obtained from the Green function. If we denote the outgoing Green propagator by $G^+(x,x';k)$, then

$$t(k)=2ikG^+(0,x_0;k)e^{-ikx_0}\ . \tag{3}$$

We assume coherent, dissipationless transport and we neglect the effects of charge accumulation. Quasi-one-dimensional dynamics is assumed, which may be realized in the lowest subband of a very narrow quantum wire.

The body of this paper is organized as follows: Double-barrier resonant tunneling is reviewed and discussed in Sec. II. A general treatment of quantum waveguides with attached resonators is presented in Sec. III, which includes the proof for the existence of transmission zeros as a consequence of unitarity. We study thin-wire networks in Sec. IV and show results for various t-stub structures. Section V contains concluding remarks.

II. DOUBLE-BARRIER RESONANT TUNNELING

It is well known that transmission resonances occur in double-barrier resonant-tunneling structures,[63,64] and

that these resonances are related to the existence of quasibound states in the quantum-well region. This relationship can be made explicit when viewing the transmission amplitude in the complex-energy plane.[65,66] It has been shown that the poles of the propagator are the same as the poles of the transmission amplitude.[66] Consequently, a quasibound state at energy E_0 and decay time $\tau=\hbar/\Gamma$ gives rise to a simple pole in the transmission amplitude $t(z)$ at the complex energy $z=E_0-i\Gamma/2$. If this pole is sufficiently close to the real-energy axis, the transmission probability $T(E)=|t(E)|^2$ for a physical energy on the real-energy axis E is given by

$$T(E)=\frac{\frac{1}{4}\Gamma^2}{(E-E_0)^2+\frac{1}{4}\Gamma^2}\ , \tag{4}$$

which is a Lorentzian line centered at energy E_0 with a full width at half maximum of Γ. This Breit-Wigner formula[67,68] describes the transmission resonance which is caused by the quasibound state at energy E_0 and decay time $\tau=\hbar/\Gamma$.

It is instructive to demonstrate how a quasibound state, which is the constructive superposition of multiply reflected waves, gives rise to a pole in the complex-energy plane. In analogy to an optical Fabry-Pérot resonator,[69] the total transmission amplitude $\mathcal{T}$ can be expressed in terms of the partial transmission and reflection amplitudes, t's and r's, at each barrier. For transmission from left to right,

$$\mathcal{T}_{RL}=t_{RW}(e^{ikL}+e^{ikL}r_Re^{ikL}r_Le^{ikL}+e^{ikL}r_Re^{ikL}r_Le^{ikL}r_Re^{ikL}r_Le^{ikL}+\cdots)t_{WL}\ , \tag{5a}$$

$$=t_{RW}\frac{1}{e^{-ikL}-r_Re^{ikL}r_L}t_{WL}\ . \tag{5b}$$

Here, t_{WL} and t_{RW} denote the transmission amplitudes from the left to the well region and from the well region to the right, respectively. The reflection amplitudes at the right and the left barriers are denoted by r_R and r_L, respectively. An electron with energy E and wave number $k=\sqrt{(2m^*E)/\hbar^2}$ accumulates a phase factor of $\exp(ikL)$ in traversing the width of the well, which is denoted by L. Poles in the transmission amplitude are thus possible at those energies and wave numbers for which the resonance denominator in Eq. (5b) vanishes. It is an easy matter to see that, for real-valued reflection amplitudes, this occurs for wave numbers k with a real part which is an integer multiple of π/L. But this also is precisely the condition which determines the energies of the quasibound states. Therefore, transmission resonances and resonant states coincide in energy. We also emphasize that the geometric series in Eq. (5a) does not possess zeros (except for the trivial case of zero transmission, i.e., $t_{WL}=0$ or $t_{RW}=0$.)

We illustrate the above arguments with a numerical example. Figure 1 shows the transmission coefficient in the complex-energy plane for a double-barrier resonant-tunneling system which is schematically depicted in the inset (barrier height $V_0=0.2$ eV, barrier depth $V_W=-0.1$ eV, well width $L=30$ nm, and barrier thickness $b=5$ nm). This structure supports true bound states for $V_W<E<0$, quasibound states for $0<E<V_0$, and continuum resonances for $E>V_0$. Part (a) of Fig. 1 shows the transmission probability on the real-energy axis ($E>0$), while part (b) depicts a contour plot of the absolute value of the transmission amplitude in the complex-energy plane. Energies are given in units of the first transmission peak $E_1=28.2$ meV. Note that transmission resonances and poles occur at essentially the same real energies and that no transmission zeros exist. The lowest three resonances possess energies below the barrier height; they correspond to long-lived states with poles close to the real-energy axis. The continuum resonances at higher energies have shorter lifetimes and the corresponding poles move farther into the complex-energy plane. Alternately, increasing the strength of the barrier (height or thickness) moves the poles closer up to the real-energy axis, which implies a longer lifetime of the resonant state. In the limit of an infinite barrier, only bound states exist and the poles move onto the real axis at these bound-state energies.

Figure 2(a) shows the charge accumulated in the quantum well, which is obtained as the integral of the charge density between the barriers; the location of each pole is indicated by an arrow. Consistent with our interpretation, maximum accumulation is found at those energies which correspond to the quasibound states. The resonant charge buildup is due to the constructive superposition of reflected and transmitted waves.

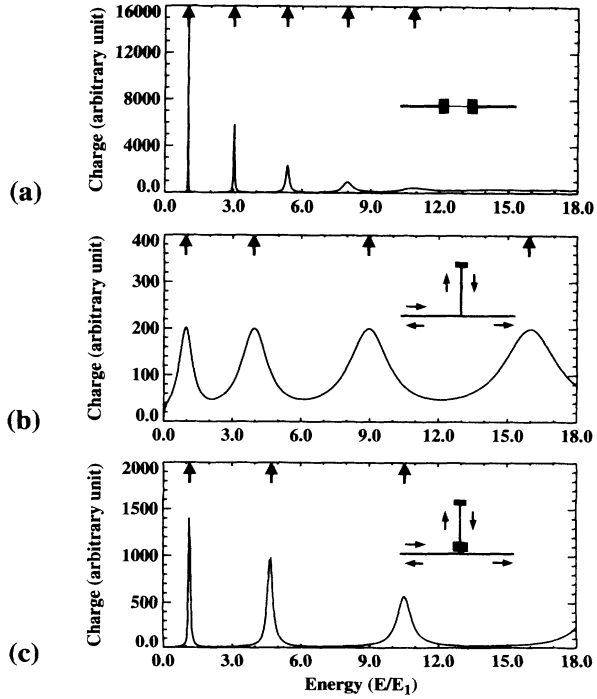

FIG. 2. Charge accumulated in the (a) well region for double-barrier resonant tunneling (same parameters as in Fig. 1), (b) strongly coupled t stub (same parameters as in Fig. 4), and (c) weakly coupled t stub (same parameters as in Fig. 5). In each case, the arrows indicate the positions of the poles.

III. QUANTUM WAVEGUIDES WITH ATTACHED RESONATORS

It is well known that the transmission coefficient in a quantum waveguide possesses structure due to changes in the waveguide geometry, such as bends, constrictions, crosses, etc. The related problem of conduction in waveguides in the presence of quasibound states has received less attention, although a few studies have been reported.[22,23] Here, we specifically focus on transmission in quantum waveguide structures which are connected to resonant cavities. The isolated resonator possesses bound states; attaching it to the conduction channel allows the wave function to leak out. We will show that this coupling introduces both finite lifetimes of the quasibound states and resonance effects in the transmission probability. These features are similar to the double-barrier resonant-tunneling problem considered in the previous section; however, the structure of the transmission amplitude in the complex-energy plane is different in the present case. In particular, we will demonstrate that transmission zeros exist for the resonant waveguides, and that the complex transmission amplitude possesses zero-pole pairs which are related to the quasibound states.

Coupling between the quantum waveguide and the resonator is accomplished in two steps, as schematically shown in Fig. 3. First, the junction region is viewed as the branch point in a three-way splitter, as indicated by the dashed line in Fig. 3(a). The properties of this wire branch are described by a scattering matrix, which is further explained in Sec. III A. Second, the resonator is obtained by closing off the sidearm, as schematically shown in Fig. 3(b). The standing wave in the resonant cavity is characterized by a phase factor, which is detailed in Sec. III B. Based on the unitarity of the scattering matrix, we are able to prove that the transmission probability for these structures exhibits zeros.

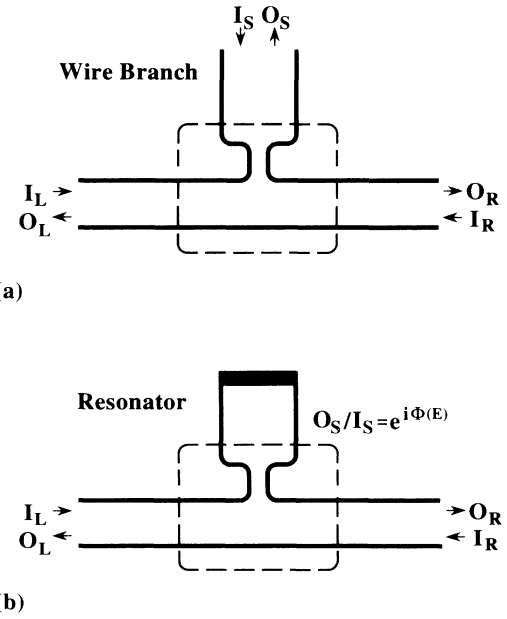

FIG. 3. Schematic drawing of a waveguide with a resonantly coupled cavity; (a) shows a wire branch with incoming and outgoing waves outside the junction region, which is indicated by the dashed box; (b) shows a resonant t stub which is obtained by closing off the sidearm.

A. Wire branch

For the three-way splitter, as shown in Fig. 3(a), the amplitudes of outgoing and incoming waves are related by the 3×3 scattering matrix

$$\begin{bmatrix} O_L \\ O_R \\ O_S \end{bmatrix} = \begin{bmatrix} r_L & t_{LR} & t_{LS} \\ t_{RL} & r_R & t_{RS} \\ t_{SL} & t_{SR} & r_S \end{bmatrix} \begin{bmatrix} I_L \\ I_R \\ I_S \end{bmatrix} . \tag{6}$$

The elements of the scattering matrix represent the reflection amplitudes in each branch, the r's, and the transmission amplitudes between the various arms, the t's; the branches are denoted by L, R, and S, for left, right, and side (or stub), respectively. We have implicitly assumed single-mode behavior, i.e., there is only one relevant transverse mode in each branch to scatter to. Time-reversal invariance, which applies here in the absence of magnetic fields, constrains the scattering matrix to be symmetric.[70,71] Current conservation requires this scattering matrix also to be unitary, which implies relationships between the various reflection and transmission amplitudes given in Appendix A.

The values of the elements in the scattering matrix depend upon both the carrier energy and the junction geometry. This, of course, offers us the possibility of controllable device operation. For the special case of a completely symmetrical three-way splitter with three identical arms, the scattering matrix is constant, which will be shown below. Generally, the transmission and reflection amplitudes for a branch are slowly varying functions of energy.

B. Resonator

Terminating the sidearm completely results in the formation of a standing wave in the stub. The amplitudes of the outgoing and incoming waves then no longer are linearly independent, but are constrained by an additional relationship,

$$O_S = \lambda(E) I_S . \tag{7}$$

Here, $\lambda = \exp[i\Phi(E)]$ is a phase factor which describes the standing wave. The energy-dependent phase $\Phi(E)$ depends upon the details of the resonator geometry.

Transmission in the presence of the resonator is described by a 2×2 scattering matrix. The condition (7) reduces the dimensionality of the original S matrix by 1. Combining Eqs. (6) and (7), it is an easy matter to show that,

$$\begin{bmatrix} O_L \\ O_R \end{bmatrix} = \begin{bmatrix} \mathcal{R}_L & \mathcal{T}_{LR} \\ \mathcal{T}_{RL} & \mathcal{R}_R \end{bmatrix} \begin{bmatrix} I_L \\ I_R \end{bmatrix} , \tag{8}$$

where $\mathcal{T}_{RL}$ denotes the transmission amplitude from left to right, and $\mathcal{R}_L$ the reflection amplitude for the left-hand side, which are given by

$$\mathcal{T}_{RL}=t_{RL}+\frac{t_{RS}t_{SL}}{\lambda-r_S}\ , \tag{9}$$

$$\mathcal{R}_L=r_L+\frac{t_{SL}t_{SL}}{\lambda-r_S}\ . \tag{10}$$

Note that the total amplitudes depend upon the characteristics of the t-stub resonator, i.e., $\lambda(E)$, and the details of the three-way splitter, i.e., the partial amplitudes $t(E)$ and $r(E)$. In a fashion similar to double-barrier resonant tunneling, the second term of Eq. (9) can be expanded as

$$\mathcal{T}_{RL}=t_{RL}+t_{RS}\left[\frac{1}{\lambda}+\frac{1}{\lambda}r_S\frac{1}{\lambda}+\frac{1}{\lambda}r_S\frac{1}{\lambda}r_S\frac{1}{\lambda}+\cdots\right]t_{SL}\ . \tag{11}$$

The resulting geometric series, contained in the brackets, describes multiple reflections in the sidearm. Each round-trip in the stub (up and down) contributes a phase factor $1/\lambda$, and each reflection back into the stub a factor r_S. The amplitudes for being scattered into (from the left) and out (to the right) of the resonator are denoted by t_{SL} and t_{RS}, respectively, and t_{RL} denotes the straight-through transmission path without a detour into the resonant stub.

The general form of $\mathcal{T}_{RL}$ is that it consists of two independent terms, as seen in Eqs. (9) and (11). One term describes the straight-through transmission in the absence of the stub, and the second term is a geometric series which is due to multiple reflections in the resonator. This has as a consequence the following structure of the transmission amplitude in the complex-energy plane: (i) poles are possible because of the resonance denominator, in analogy to double-barrier resonant tunneling; and (ii) zeros are possible because the two terms may cancel each other. The existence of both terms is the major difference from double-barrier resonant tunneling. In the latter case, as discussed in the previous section, the transmission amplitude is given by a single term, which represents the geometric series.

The form $\lambda-r_S$ for the denominator of $\mathcal{T}_{RL}$ also predicts that the sharpness of the resonance features will depend upon the strength of the coupling between the sidearm and the channel. For a weakly coupled t stub, there is a large probability for reflection back into the sidearm, i.e., $|r_S|\to 1$. This implies that in this case r_S may approach λ on the unit circle, thus giving rise to sharp resonance features. On the other hand, a strongly coupled t stub has $|r_S|=\frac{1}{3}$ and therefore the amplitude r_S never gets close to λ on the unit circle, resulting in weak features in the transmission coefficient.

C. Proof of the existence of transmission zeros

In the previous section we demonstrated that transmission zeros are possible, in principle. In this section we prove that, in fact, transmission zeros must occur and that their existence is a consequence of unitarity.

A zero of the transmission amplitude at a certain energy means that $\mathcal{T}_{RL}=0$ for that energy. As can be seen from Eq. (9), this implies that

$$\lambda=r_S-\frac{t_{RS}t_{SL}}{t_{RL}}\quad(\text{when } \mathcal{T}_{RL}=0)\ . \tag{12}$$

The above condition relates a property of the resonator, the phase factor λ, to a property of the junction between the waveguide and the resonant cavity, the t's and r's which are the elements of the scattering matrix for the three-way splitter. Because λ is a phasor on the unit circle, Eq. (12) can only be true if the right-hand side also lies on the unit circle for those energies at which transmission zeros occur. It is a perhaps surprising consequence of unitarity that *for all energies* the right-hand side of Eq. (12) is constrained to be on the unit circle, i.e., *always*

$$\left|r_S-\frac{t_{RS}t_{SL}}{t_{RL}}\right|=1\ . \tag{13}$$

The detailed proof of the above equation is given in Appendix A. Unitarity, therefore, ensures that both the left- and the right-hand side of Eq. (12) are constrained to the unit circle, which implies that a transmission zero occurs when both phase angles are the same. Usually, the right-hand side is a slowly varying function of energy, and the left-hand side is a phasor which moves around the unit circle with an angular dependence proportional to the wave number, as shown in the examples below.[72]

Using similar arguments, one may also investigate the conditions for unity transmission, $\mathcal{T}_{RL}=1$. The unitarity of the scattering matrix by itself is not sufficient to ensure the existence of 1s in the transmission amplitude. As shown in Appendix A, $\mathcal{T}_{RL}=1$ holds true for certain energies if the structure is symmetric with respect to "left" and "right," i.e., if the scattering matrix possesses the symmetry property that $t_{RS}=t_{LS}$, etc. This behavior is similar to double-barrier resonant tunneling, where it is known that perfect transmission only occurs for symmetric barrier structures.[63,66]

IV. THIN-WIRE NETWORKS

We illustrate the above general arguments by demonstrating several specific examples. As a model system, we choose networks of thin wires which are sufficiently narrow that only motion in the direction of the wires is of interest. The motion perpendicular to the wire is frozen in the lowest transverse subband, resulting in quasi-one-dimensional dynamics. These thin-wire networks exhibit the essential behavior of the transmission amplitude in the complex-energy plane under study here, without additional geometric complications inherent in a true two-dimensional system. For certain structures our model is sufficiently simple to yield analytical answers. Other cases require numerical investigation. We show results for a variety of so-called strongly and weakly coupled stubs.

A. Three-way splitter

The basic building block of the stub structures is the simple wire branch, or three-way splitter. The wave functions in the left, right, and stub branches are denoted

by Ψ_L, Ψ_R, and Ψ_S, respectively. For a perfect wire, they are superpositions of incoming and outgoing plane waves,

$$\Psi_L = I_L e^{ikx_L} + O_L e^{-ikx_L} , \tag{14a}$$

$$\Psi_R = O_R e^{ikx_R} + I_R e^{-ikx_R} , \tag{14b}$$

$$\Psi_S = O_S e^{ikx_S} + I_S e^{-ikx_S} . \tag{14c}$$

Here, x_L, x_R, and x_S denote the spatial coordinates in each branch, i.e., left, right, and stub, respectively. The matching conditions at the branch point, $x_L = x_R = x_S = 0$, for the wave functions and the derivative are

$$I_L + O_L = O_R + I_R , \tag{15a}$$

$$I_L + O_L = O_S + I_S , \tag{15b}$$

$$I_L - O_L = O_R - I_R + O_S - I_S . \tag{15c}$$

The last of these relations is the matching condition for the derivatives. We require the sum of the derivatives in all directions at a branch point to be equal to zero, which is a generalization of the current-conservation condition. However, the above derivative condition is stronger than current conservation; it implies the conservation of current, but not vice versa.[73]

The above system of equations represents three conditions which constrain the six amplitudes for the incoming and outgoing waves in each of the three branches. These six amplitudes are also related by a scattering matrix when viewing the three amplitudes of the incoming waves as independent parameters, and the three amplitudes of the outgoing waves as the dependent variables. The three equations (15) thus are sufficient to completely specify the scattering matrix. It is an easy matter to show that,

$$\begin{bmatrix} O_L \\ O_R \\ O_S \end{bmatrix} = \begin{bmatrix} -\frac{1}{3} & \frac{2}{3} & \frac{2}{3} \\ \frac{2}{3} & -\frac{1}{3} & \frac{2}{3} \\ \frac{2}{3} & \frac{2}{3} & -\frac{1}{3} \end{bmatrix} \begin{bmatrix} I_L \\ I_R \\ I_S \end{bmatrix} . \tag{16}$$

Comparing with Eq. (6), we see that $r_L = r_R = r_S = -\frac{1}{3}$ and $t_{RL} = t_{RS} = t_{SL} = \frac{2}{3}$ for this simple three-way splitter, and that the elements of the scattering matrix are independent of energy. In Appendix B, we show that the above result for the scattering matrix is a special case of previous work[13,41,44] in which the coupling of a ring to a lead was studied.

B. t stubs

We now create a t-stub resonator in the form of a dangling wire of length L by truncating the sidearm of the three-way splitter with an infinite potential barrier at $x_S = L$. The wave function has to be zero at the end of the sidearm, $O_S e^{ikL} + I_S e^{-ikL} = 0$, which implies that the amplitudes of the incoming and outgoing waves are related by a phase factor $\lambda = O_S / I_S$, as previously discussed. For this geometry, the standing waves in the resonator are characterized by the phasor $\lambda(E) = -\exp(-2ikL)$, with a phase that changes linearly with wave number k.

The transmission amplitude for this so-called strongly coupled stub, which is schematically shown in the inset of Fig. 4, can now be found by using in Eq. (9) the above form for λ and the elements of the scattering matrix for the wire branch, Eq. (16). It is an easy matter to show that the transmission amplitude is given analytically by

$$\mathcal{T} = \left[1 + \frac{i}{2} \cot(kL) \right]^{-1} . \tag{17}$$

Figure 4 shows the transmission amplitude in the complex-energy plane for a strongly coupled t stub with stub length $L = 10$ nm; part (a) shows the transmission probability on the real-energy axis, and part (b) shows a contour plot of the absolute value of the transmission amplitude in the complex-energy plane. Note the appearance of transmission zeros on the real-energy axis, and the existence of transmission poles in the complex-energy plane. The zeros occur at energies for which standing waves form in the stub, i.e., when $k = n\pi/L$ with $n = 1, 2, \ldots$. [The energy for $n = 1$, $E_1 = \hbar^2\pi^2/(2m^*L^2) = 56.2$ meV, is used as the unit of energy; note that these relative units may be used to scale the problem to different stub lengths.] The wave function at a transmission zero has to be zero at the branch point, which forces the wave function in the resonator to be zero at both ends of the stub. *Note also that the maxima of the transmission coefficient do not align with the location of the poles, as in the case of double-barrier resonant tunneling.* The most striking feature of Fig. 4 is the

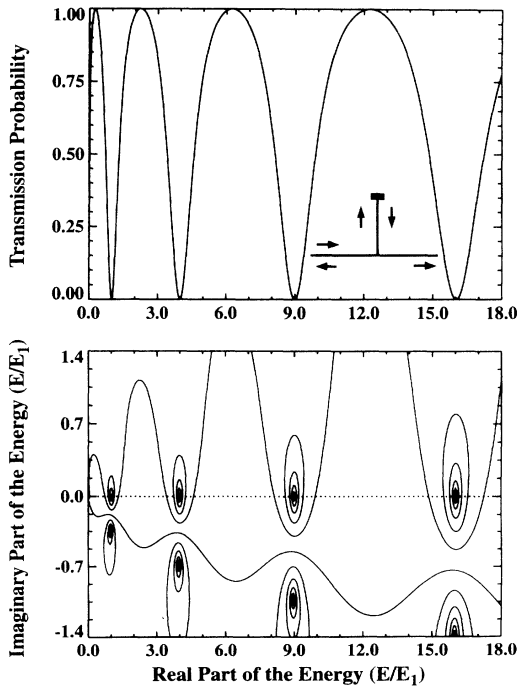

FIG. 4. Transmission coefficient for the strongly coupled t-stub structure which is schematically depicted in the inset; (a) shows the transmission probability on the real-energy axis and (b) shows a contour plot of the absolute value of the transmission amplitude in the complex-energy plane.

demonstration of zero-pole pairs in the complex-energy plane.

Because of the symmetry of the structure, transmission maxima in this case are transmission 1s. For $\mathcal{T}=1$, the wave function at the branch point must be 1, which implies a standing wave in the stub with a maximum at the branch point and a zero at the end point; i.e., when $k=(2n+1)\pi/(2L)$ with $n=0,1,2,\ldots$. In general, maxima for waveguide structures occur between two zeros at some intermediate energy which is determined by the proximity to the real-energy axis of neighboring poles. For this simple case, the elements of the scattering matrix are constants, i.e., independent of energy. The energy dependence of the transmission amplitude is provided by the resonance phasor $\lambda(E)$.

An energy dependence in the elements of the scattering matrix may be introduced by weakly coupling the stub to the channel via a tunneling barrier of length l and height V_0, as schematically depicted in the inset of Fig. 5. The transmission amplitude may be given in closed form,

$$\mathcal{T}=\left[1+\frac{i}{2}\frac{K}{k}\frac{[k\cos(k\Delta)\cos(Kl)-K\sin(k\Delta)\sin(Kl)]}{[k\cos(k\Delta)\sin(Kl)+K\sin(k\Delta)\cos(Kl)]}\right]^{-1}, \tag{18}$$

where $k=\sqrt{2m^*E}/\hbar$, $K=\sqrt{2m^*(E-V_0)}/\hbar$, and $\Delta=L-l$. For the example shown in Fig. 5, we choose a tunneling barrier at the branch point with a height of 0.5 eV and a thickness of 1 nm (the same dimensions will also be used for the barriers in subsequent examples). Figure 5 depicts the transmission amplitude in the complex-energy plane for this so-called weakly coupled stub. As before, the energy is expressed in units of $E_1=\hbar^2\pi^2/(2m^*L^2)=56.2$ meV. Note again the existence of transmission zeros on the real-energy axis, as predicted by our general arguments in Sec. III. Note also that, with respect to the previous example of a strongly coupled stub, the poles in the complex plane now are closer to the real axis, which corresponds to the longer lifetime of the resonant states due to the confining barrier. As a consequence of the zeros and poles approaching each other in the complex plane, the maxima on the real axis move close to the zeros, which results in the stronger energy dependence observed in Fig. 5(a) when compared to Fig. 4(a). Each resonant state produces a zero-pole pair in the complex-energy plane, which gives rise to the observed energy dependence of the transmission coefficient on the real-energy axis. With increasing barrier height, the pole approaches the zero, which leads to a sharper and sharper transition between a transmission 0 and 1 on the real-energy axis. In the limit of an infinitely high barrier, the poles and zeros merge, which corresponds to unity transmission probability, and independent of energy, for a channel with a completely decoupled stub.

The proximity of transmission 0's and 1's on the real-energy axis, which results in the more or less sharp variations of the transmission coefficient with energy, can be understood from a wave-function argument. The electronic states in the resonator are standing waves, which have to match to the wave functions in the channel at the branch point. This implies that for a transmission 0 or 1, the wave function at the branch point has to be 0 or 1, respectively. This circumstance is illustrated in Fig. 6, where the branch point is labeled by 0 on the spatial coordinate. Shown are the absolute values of the wave functions in the stub at both transmission 0's and 1's for the cases of strongly and weakly coupled t stubs, respectively. As discussed above, and illustrated in Fig. 6(a), for the strongly coupled stub the standing waves in the resonator differ by a quarter wavelength for $\mathcal{T}=0$ and $\mathcal{T}=1$. This implies that in this case the 0s and 1s are well separated in energy, as seen in Fig. 4(a). For the weakly coupled stub, the standing wave is connected to the wire branch via a tunneling barrier, as illustrated in Fig. 6(b). Now only a small change in the wavelength of the standing wave is needed as the transmission coefficient varies from a maximum to a minimum. Also note that the amplitudes of the standing waves at a 0 are larger than those at a 1. Figures 2(b) and 2(c) illustrate, as a function of energy, the charge buildup in the t-stub

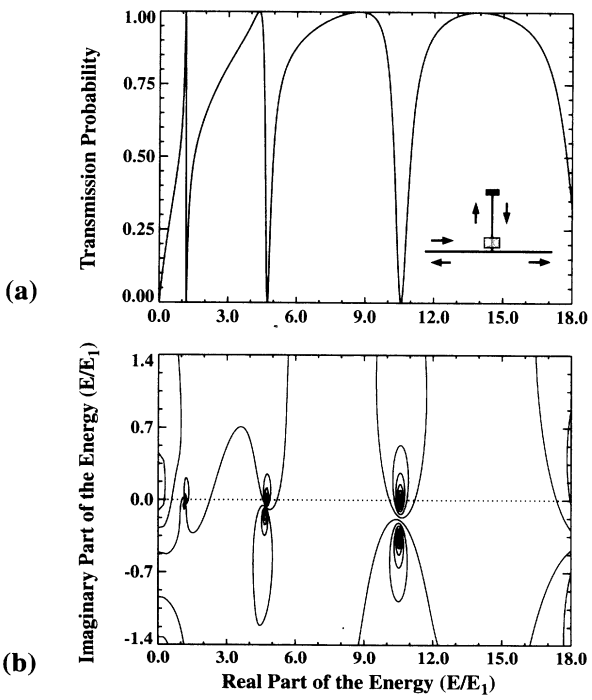

FIG. 5. Transmission coefficient for the weakly coupled t-stub structure which is schematically depicted in the inset; (a) shows the transmission probability on the real-energy axis and (b) shows a contour plot of the absolute value of the transmission amplitude in the complex-energy plane.

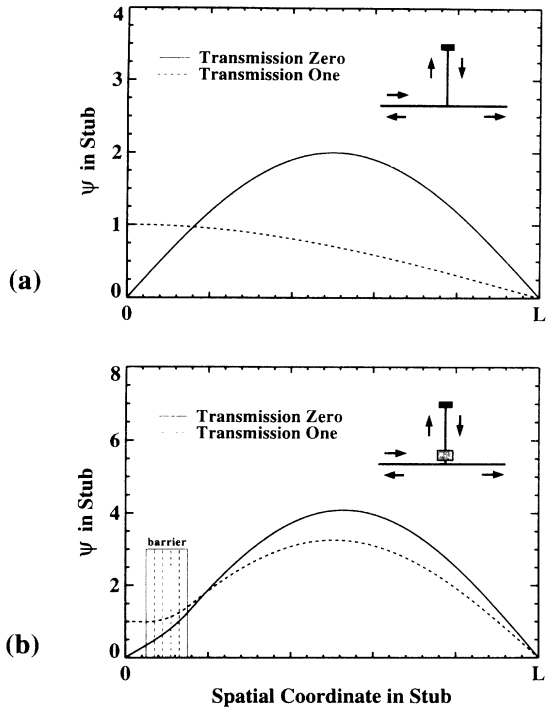

FIG. 6. Wave functions in the stubs corresponding to the lowest transmission 0 (solid line) and transmission 1 (dotted line) for the t-stub structures shown in the insets; (a) strongly coupled t stub (same parameters as in Fig. 4) and (b) weakly coupled t stub (same parameters as in Fig. 5).

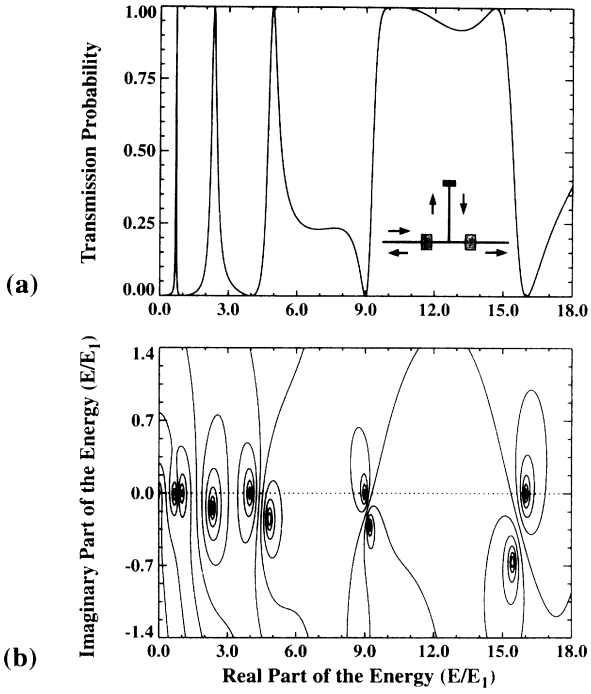

FIG. 7. Transmission coefficient for DBRT in addition to the strongly coupled t-stub structure which is schematically depicted in the inset; (a) shows the transmission probability on the real-energy axis and (b) shows a contour plot of the absolute value of the transmission amplitude in the complex-energy plane.

structures, which is measured by the integral of $|\Psi|^2$ over the length of the stub. The arrows at the top axis denote the locations of the poles of the transmission amplitude in the complex-energy plane for the cases of strongly and weakly coupled stubs, which are identified in the insets; compare also Figs. 4(b) and 5(b). The resonant states for the weakly coupled stub are sharper in energy and they contain more charge than those of the strongly coupled stub, which is due to the confinement provided by the tunneling barrier. Note that, as for the case of double-barrier resonant tunneling, the location of the charging peaks is determined by the poles.

It is interesting to study double-barrier resonant tunneling in addition to t-stub resonances. The results of adding two tunneling barriers on the transmission channel for strongly and weakly coupled stubs are shown in Figs. 7 and 8, respectively. The separation between these two barriers with height $V_0=0.5$ eV is assumed to be $d=4$ nm, and the length of the stub is again $L=10$ nm. As in the previous example, the energy is expressed in units of $E_1=\hbar^2\pi^2/(2m^*L^2)=56.2$ meV. We notice in both cases that there is, in addition to the now familiar zero-pole pairs, another set of poles in the complex-energy plane, and a corresponding set of transmission 1s on the real-energy axis. The additional 1s are caused by resonant tunneling through the two tunneling barriers on the transmission channel, in complete analogy to the previously discussed case of double-barrier resonant tunneling. Comparing Figs. 4 and 7 for the strongly coupled

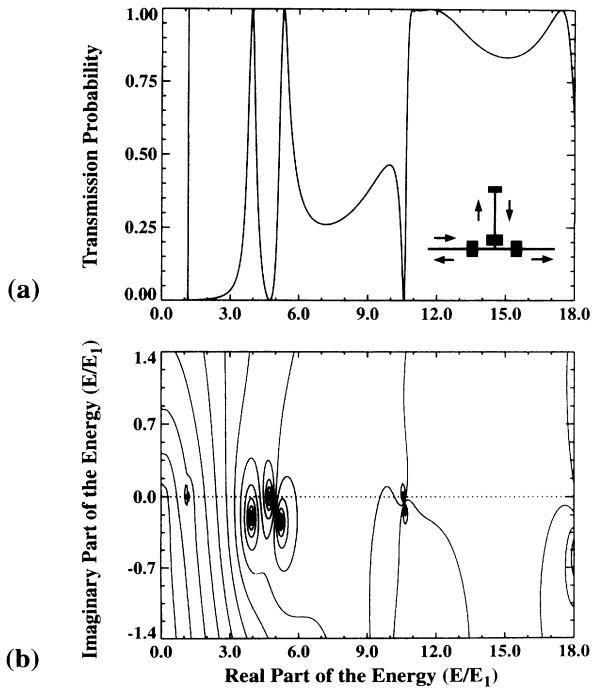

FIG. 8. Transmission coefficient for DBRT in addition to the weakly coupled t-stub structure which is schematically depicted in the inset; (a) shows the transmission probability on the real-energy axis and (b) shows a contour plot of the absolute value of the transmission amplitude in the complex-energy plane.

stub, we note that the transmission zeros occur at exactly the same energies. Because of the confinement provided by the barriers, the zero-pole pairs are closer together in Fig. 7 than in Fig. 4, which is also reflected in the sharper energy dependence on the real-energy axis. The additional pole at $E=0.14$ eV, which is associated with the transmission 1, is due to the energy of the first resonant state of two tunneling barriers on the transmission channel. Because of our choice for the separation between the barriers and the length of the stub, this energy is close to the energy of the second-lowest t-stub resonant state. This leads to the apparent coupling of the two poles, and the resulting "stretching" of the second-lowest zero-pole pair. The case of the weakly coupled stub with double barriers on the transmission channel is illustrated in Fig. 8; compare to Fig. 5 without the barriers in the channel. Again, the additional double-barrier resonant tunneling does not alter the location of the zeros which are a property of the quasibound states in the stub, cf. Figs. 8 and 5. Also, the additional barriers lead to the very close zero-pole pairs and sharp transmission peaks shown in Fig. 8. Because of the relative lengths chosen, the lowest double-barrier resonant state is close in energy to the second-lowest quasibound state in the t stub. As also explained above, this leads to an interaction between the pole which is due to double-barrier resonant tunneling, and the pole which belongs to the t-stub's zero-pole pair.

All wire structures discussed so far are symmetrical about the t stub, which implies that the scattering matrix possesses a left-right invariance. As shown in the previous figures and proven in the Appendix, this symmetry property ensures that transmission maxima are transmission 1s. Nonsymmetrical wire structures are shown in the insets of Figs. 9 and 10 for strongly and weakly coupled t stubs, respectively. The left-right symmetry is broken by placing a single tunneling barrier on one side of the transmission channel at a distance of $d=2$ nm from the branch point. While transmission maxima no longer correspond to perfect transmission, $\mathcal{T}<1$, transmission zeros still persist in accordance with our theory. Note, furthermore, that the asymmetrical barrier in the channel does not alter the location of the zeros, which is a property of the t stub; compare Fig. 9 to Fig. 4 (strong coupling), and Fig. 10 to Fig. 5 (weak coupling). For the strongly coupled t stub, there are poles in the complex-energy plane which correspond to standing waves between the tunneling barrier and the end of the stub. An example is the additional pole between the lowest and second-lowest zero-pole pair shown in Fig. 9. For the weakly coupled t stub, these additional quasibound states are not possible because of the barrier at the branch point. Consequently, Fig. 10 does not show double-barrier resonant-tunneling poles in addition to the familiar zero-pole pairs.

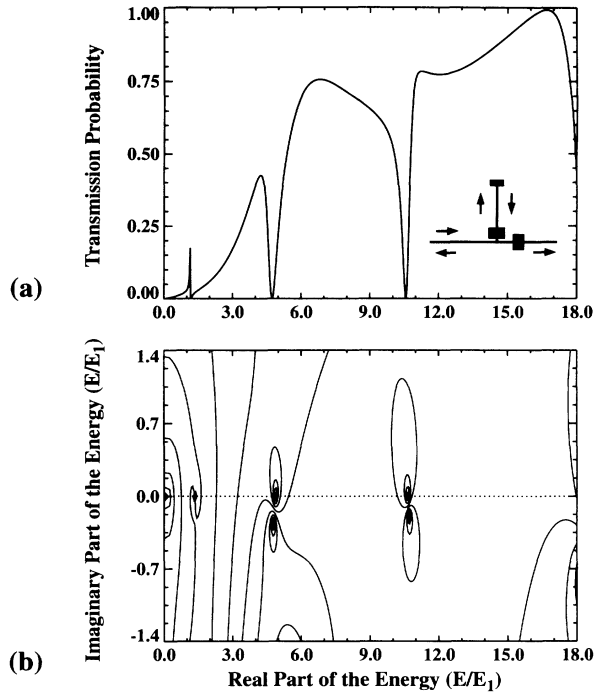

FIG. 10. Transmission coefficient for the asymmetrical t-stub structure which is schematically depicted in the inset; (a) shows the transmission probability on the real-energy axis and (b) shows a contour plot of the absolute value of the transmission amplitude in the complex-energy plane.

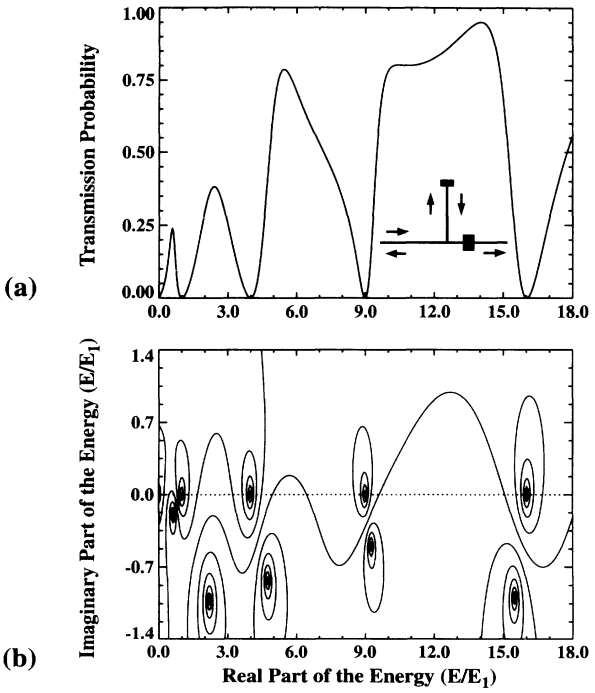

FIG. 9. Transmission coefficient for the asymmetrical t-stub structure which is schematically depicted in the inset; (a) shows the transmission probability on the real-energy axis and (b) shows a contour plot of the absolute value of the transmission amplitude in the complex-energy plane.

V. CONCLUSION

We have studied transmission phenomena in quantum waveguide systems in the presence of resonant cavities. In particular, we have investigated the analytical

behavior of the transmission amplitude in the complex-energy plane. For the single-mode quantum wires under study here, the dynamics is quasi-one-dimensional. This also allows us to compare directly the much studied problem of double-barrier resonant tunneling to the less well understood case of transmission in quantum-wire systems; DBRT can be viewed as transmission in a channel which also contains both barriers. One of our main conclusions is that the analytic behavior of the transmission amplitude is different depending upon whether or not the resonant cavity is part of the transmission channel, as for DBRT, or is attached to the channel, as for the t stubs. If the main transmission path is directly through the resonator, the transmission amplitude only exhibits poles in the complex-energy plane. These poles give rise to the well-known Lorentzian-shaped Breit-Wigner transmission resonances. If in addition to the direct transmission path there is an additional path due to an attached resonator, the transmission amplitude exhibits zero-pole pairs in the complex-energy plane. The vicinity of these zeros and poles produces resonance-antiresonance behavior of the transmission coefficient.

It was noted by several workers in previous studies that the transmission coefficient in quantum waveguide systems exhibited a qualitatively different behavior as compared to the familiar case of DBRT. Our research shows that these observed sharp variations of the transmission coefficient as a function of energy can be understood in terms of the zero-pole pairs in the complex-energy plane. The proximity of the zero and the pole which is produced by each quasibound state leads to the sharp energy dependence. Furthermore, we showed that the existence of transmission zeros for resonantly coupled waveguides is a consequence of unitarity, regardless of the symmetry of the system. In other words, reflection peaks with amplitude equal to 1 occur for symmetrical as well as for nonsymmetrical structures. In contrast, transmission peaks with an amplitude equal to 1 only occur for symmetrical structures. This result is familiar from DBRT, where it is known that perfect transmission is possible only for symmetrical barriers. In related studies, Price[74] distinguishes between peaks in transmission, which he terms resonances of the first kind, and dips in the transmission coefficient, which he terms resonances of the second kind. He also shows that the peak value of the reflection probability, corresponding to the resonances of the second kind, is always 1, regardless of the symmetry of the system, in contrast to the transmission-resonance case (resonances of the first kind). This behavior is shown to persist in the case of multichannel ballistic transport.[75] In a related paper,[76] we point out that Price's resonances of the second kind are a special case of the zero and the pole coinciding in energy. In general, the zero-pole pairs produce resonance-antiresonance features and not either resonances or dips.

Another striking difference between DBRT and the waveguides is the location of the transmission peaks relative to the poles in the complex-energy plane. From DBRT, one is used to associate the location of a transmission maximum with the energy of a quasibound state, which are represented by the poles. For transmission in waveguides with attached resonators, the quasibound states still are given by the poles in the complex-energy plane; however, their location does *not* match the peaks in the transmission probability. Each quasibound state now is represented by a zero-pole pair, where the energy of the pole is close to the energy of the zero. Transmission maxima occur somewhere between the zeros, where the exact location of the peaks depends upon the proximity of the poles to the zero and to the real-energy axis. Therefore, it is no longer valid for the quantum waveguide structures to associate the energy of a transmission peak with the energy of a quasibound state.

We can interpret our findings in the context of Fano resonances,[51] which are known to occur when two scattering channels are available, one corresponding to a continuum of states and the other to a discrete quasibound state. Our work shows that the transmission amplitude exhibits zero-pole pairs in the complex-energy plane when there is continuum transmission in addition to a resonant path. Upon studying the line shape of a resonance-antiresonance feature,[76] we were able to demonstrate that, in fact, Fano resonances correspond to a zero-pole structure in the complex-energy plane.

In summary, our main conclusions are: (i) Transmission zeros exist in quantum waveguide structures with attached resonators, and their existence is a consequence of unitarity; this result is in contrast to DBRT where no transmission zeros are possible. (ii) For the quantum waveguide structures, each quasibound state of the attached resonator leads to a zero-pole pair of the transmission amplitude in the complex-energy plane. (iii) In a fashion similar to DBRT, symmetrical waveguide systems possess peaks with perfect transmission. (iv) In contrast to DBRT, the location of the transmission maxima in resonantly coupled quantum waveguides does not coincide with the energy of the quasibound resonator states.

ACKNOWLEDGMENTS

We are grateful for stimulating discussions with Dr. M. Büttiker, M. Chen, Dr. S. M. Goodnick, H. K. Harbury, M. Leng, Dr. W. Pötz, Dr. P. Price, and Dr. M. Sain. This work was supported, in part, by the Air Force Office of Scientific Research and the Office of Naval Research.

APPENDIX A: UNITARITY AND ZEROS

1. Proof of the existence of transmission zeros

In this section, we prove that, for all energies,

$$\left| r_S - \frac{t_{RS} t_{SL}}{t_{RL}} \right| = 1 \ , \tag{A1}$$

which ensures the existence of transmission zeros.

Let $\alpha = r_S - t_{RS} t_{SL} / t_{RL}$. We will prove (A1) by demonstrating that $\alpha \alpha^* = 1$.

$$\alpha\alpha^* = r_S r_S^* + \frac{t_{RS}t_{RS}^* t_{SL}t_{SL}^*}{t_{RL}t_{RL}^*} - \frac{r_S^* t_{RS}t_{SL}t_{RL}^*}{t_{RL}t_{RL}^*} - \frac{r_S t_{RS}^* t_{SL}^* t_{RL}}{t_{RL}t_{RL}^*} . \quad \text{(A2)}$$

The unitarity of the scattering matrix requires

$$r_L r_L^* + t_{RL}t_{RL}^* + t_{SL}t_{SL}^* = 1 , \quad \text{(A3)}$$

$$t_{RL}t_{RL}^* + r_R r_R^* + t_{RS}t_{RS}^* = 1 , \quad \text{(A4)}$$

$$t_{SL}t_{SL}^* + t_{RS}t_{RS}^* + r_S r_S^* = 1 , \quad \text{(A5)}$$

and

$$r_L t_{RL}^* + t_{RL}r_R^* + t_{SL}t_{RS}^* = 0 , \quad \text{(A6)}$$

$$r_L t_{SL}^* + t_{RL}t_{RS}^* + t_{SL}r_S^* = 0 , \quad \text{(A7)}$$

$$t_{RL}t_{SL}^* + r_R t_{RS}^* + t_{RS}r_S^* = 0 . \quad \text{(A8)}$$

We now substitute (A7), $r_S^* t_{SL} = -(r_L t_{SL}^* + t_{RL}t_{RS}^*)$, into the third term of (A2) and the complex conjugate of (A8), $r_S t_{RS}^* = -(t_{RL}^* t_{SL} + r_R^* t_{RS})$, into the fourth term. We define β as the sum of these two terms, which is given by

$$\beta = -\frac{r_S^* t_{SL}t_{RL}^* t_{RS}}{t_{RL}t_{RL}^*} - \frac{r_S t_{RS}^* t_{RL}t_{SL}^*}{t_{RL}t_{RL}^*} ,$$

$$= \frac{r_L t_{SL}^* t_{RL}^* t_{RS} + t_{RL}t_{RS}^* t_{RL}^* t_{RS}}{t_{RL}t_{RL}^*} + \frac{t_{RL}^* t_{SL}t_{RL}t_{SL}^* + r_R^* t_{RS}t_{RL}t_{SL}^*}{t_{RL}t_{RL}^*} ,$$

$$= t_{RS}^* t_{RS} + t_{SL}^* t_{SL} + \frac{t_{SL}^* t_{RS}(r_L t_{RL}^* + r_R^* t_{RL})}{t_{RL}t_{RL}^*} . \quad \text{(A9)}$$

Substituting it back into (A2) and using (A5) and (A6) gives

$$\alpha\alpha^* = r_S r_S^* + t_{RS}^* t_{RS} + t_{SL}^* t_{SL} + \frac{t_{RS}t_{RS}^* t_{SL}t_{SL}^*}{t_{RL}t_{RL}^*} + \frac{t_{SL}^* t_{RS}(r_L t_{RL}^* + r_R^* t_{RL})}{t_{RL}t_{RL}^*} ,$$

$$= 1 + \frac{t_{RS}t_{RS}^* t_{SL}t_{SL}^*}{t_{RL}t_{RL}^*} + \frac{t_{SL}^* t_{RS}(-t_{SL}t_{RS}^*)}{t_{RL}t_{RL}^*} ,$$

$$= 1 . \quad \text{(A10)}$$

Q.E.D.

2. Proof of the existence of transmission 1s in symmetrical structures

In this section, we prove that, for a symmetrical structure,

$$\left| r_S - \frac{t_{SL}t_{SL}}{r_L} \right| = 1 , \quad \text{(A11)}$$

which ensures the existence of transmission 1s.

Instead of proving $\mathcal{T}_{RL} = 1$ directly, we prove $\mathcal{R}_L = 0$, which implies

$$\lambda = r_S - \frac{t_{SL}t_{SL}}{r_L} . \quad \text{(A12)}$$

If the modulus of the right-hand side is 1, which is condition (A11), zeros in reflection, and thus 1s in transmission, must exist.

Let $\alpha = r_S - t_{SL}t_{SL}/r_L$. Condition (A11) then requires $|\alpha| = 1$, which we will prove by demonstrating that $\alpha\alpha^* = 1$.

$$\alpha\alpha^* = r_S r_S^* + \frac{|t_{SL}|^4 - r_S^* t_{SL}^2 r_L^* - r_S (t_{SL}^2)^* r_L}{|r_L|^2} . \quad \text{(A13)}$$

We now substitute (A7), $r_S^* t_{SL} = -(r_L t_{SL}^* + t_{RL}t_{RS}^*)$, into the third term of (A13) and (A7), $r_L t_{SL}^* = -(t_{RL}t_{RS}^* + r_S^* t_{SL})$, into the fourth term. We define β as the sum of these two terms, which is given by

$$\beta = \frac{-r_S^* t_{SL}^2 r_L^* - r_S (t_{SL}^2)^* r_L}{|r_L|^2} ,$$

$$= \frac{|t_{SL}|^2 |r_L|^2 + |t_{SL}|^2 |r_S|^2 + t_{RL}t_{RS}^* (t_{SL}r_L^* + r_S t_{SL}^*)}{|r_L|^2} . \quad \text{(A14)}$$

Substituting it back into (A13) and using (A7) gives

$$\alpha\alpha^* = |r_S|^2 + |t_{SL}|^2 + |t_{RS}|^2 + \frac{|t_{SL}|^4 + |r_S|^2 |t_{SL}|^2 - |r_L|^2 |t_{RS}|^2 - |t_{RL}|^2 |t_{RS}|^2}{|r_L|^2}$$

$$= 1 + \frac{|t_{SL}|^4 + |r_S|^2 |t_{SL}|^2 - |r_L|^2 |t_{RS}|^2 - |t_{RL}|^2 |t_{RS}|^2}{|r_L|^2} . \quad \text{(A15)}$$

Using (A5) in the first two terms of the above numerator, and (A3) in the last two terms, yields

$$\alpha\alpha^* = 1 + \frac{|t_{SL}|^2(1-|t_{RS}|^2) - |t_{RS}|^2(1-|t_{SL}|^2)}{|r_L|^2} ,$$

$$= 1 + \frac{(|t_{SL}|^2 - |t_{RS}|^2)}{|r_L|^2} . \quad \text{(A16)}$$

For symmetrical systems, $|t_{SL}|^2 = |t_{RS}|^2$, which proves (A11). The symmetrical structures shown in Figs. 4, 5, 7, and 8 possess transmission 1s.

For the nonsymmetrical structures shown in Figs. 9 and 10, $|t_{SL}|^2 \neq |t_{RS}|^2$, and no transmission 1s exist. Condition (A11) is not satisfied in this case.

APPENDIX B: SCATTERING MATRIX

Here, we show that our result for the scattering matrix in thin-wire networks, which we derived in Sec. IV A, is a special case of previous work in which the coupling of a ring to a lead was studied.[13,41,44] It was shown in Ref. 41 that the scattering matrix is determined by three parameters in the form,

$$S = \begin{bmatrix} -(a+b) & \epsilon^{1/2} & \epsilon^{1/2} \\ \epsilon^{1/2} & a & b \\ \epsilon^{1/2} & b & a \end{bmatrix} . \quad \text{(B1)}$$

Unitarity imposes the following constraints,

$$(a+b)^2 + 2\epsilon = 1 , \quad \text{(B2)}$$

$$a^2 + b^2 + \epsilon = 1 . \quad \text{(B3)}$$

The parameter ϵ, which is in the range $0 < \epsilon < \frac{1}{2}$, measures the strength of the coupling between the lead and the ring. A completely detached ring corresponds to $\epsilon = 0$, and maximum coupling is assumed to occur for $\epsilon = \frac{1}{2}$.

However, we noted in previous work[13] that the strongest coupling occurs for $\epsilon = \frac{4}{9}$ (and not for $\epsilon = \frac{1}{2}$). According to (B2) and (B3), $\epsilon = \frac{4}{9}$ corresponds to the following values for the other two parameters, $a = -\frac{1}{3}$ and $b = \frac{2}{3}$. The resulting scattering matrix for these values of a and b is exactly the one derived by us in Sec. IV A, i.e., Eq. (16). We conclude that our choice of the matching conditions at the branch point leads to a scattering matrix which is a special case of the general form (B1) for the parameter value $\epsilon = \frac{4}{9}$.

[1] R. Landauer, IBM J. Res. Dev. **1**, 223 (1957); Philos. Mag. **21**, 863 (1970).
[2] M. Büttiker, Phys. Rev. Lett. **57**, 1761 (1986).
[3] R. A. Webb (unpublished).
[4] *Analogies in Optics and Micro Electronics,* edited by W. VanHaeringen and D. Lenstra (Kluwer, Dordrecht, 1990).
[5] L. Esaki and R. Tsu, IBM J. Res. Dev. **14**, 61 (1970); R. Tsu and L. Esaki, Appl. Phys. Lett. **22**, 562 (1973).
[6] T. C. L. G. Sollner, W. D. Goodhue, P. E. Tannenwald, C. D. Parker, and D. D. Peck, Appl. Phys. Lett. **43**, 588 (1983); T. C. L. G. Sollner, P. E. Tannenwald, D. D. Peck, and W. D. Goodhue, *ibid.* **45**, 1319 (1984).
[7] *Nanostructure Physics and Fabrication,* edited by M. A. Reed and W. P. Kirk (Academic, Boston, 1989).
[8] *Nanostructures and Mesoscopic Systems,* edited by W. P. Kirk and M. A. Reed (Academic, Boston, 1992).
[9] W. Porod, Z. Shao, and C. S. Lent, Appl. Phys. Lett. **61**, 1350 (1992).
[10] P. F. Bagwell and R. K. Lake, Phys. Rev. B **46**, 15 329 (1992); P. F. Bagwell, A. Kumar, and R. K. Lake, in *Quantum Effect Physics, Electronics, and Applications,* edited by K. Ismail (Hilger, Bristol, 1992).
[11] F. Sols, M. Macucci, U. Ravaioli, and K. Hess, Appl. Phys. Lett. **54**, 350 (1989); J. Appl. Phys. **66**, 3892 (1989).
[12] S. Datta, Superlatt. Microstruct. **6**, 83 (1989).
[13] S. Subramaniam, S. Bandyopadhyay, and W. Porod, J. Appl. Phys. **68**, 4861 (1990).
[14] K.-F. Berggren and Z.-L. Ji, Superlatt. Microstruct. **8**, 59 (1990).
[15] Y. Avishai and Y. B. Band, Phys. Rev. B **41**, 3253 (1990).
[16] Y. Takagaki and D. K. Ferry, J. Appl. Phys. **72**, 5001 (1992).
[17] J.-B. Xia, Phys. Rev. B **45**, 3593 (1992).
[18] H. Wu, D. W. L. Sprung, J. Martorell, and S. Klarsfeld, Phys. Rev. B **44**, 6351 (1991).
[19] J. A. Brum, Phys. Rev. B **43**, 12 082 (1991).
[20] Z.-L. Ji and K.-F. Berggren, Phys. Rev. B **45**, 6652 (1992).
[21] B. Shapiro, Phys. Rev. Lett. **50**, 747 (1983).
[22] P. J. Price, IEEE Trans. Electron Devices **39**, 520 (1992).
[23] C. S. Lent, in *Computational Electronics: Semiconductor Transport and Device Simulation,* edited by K. Hess, J. P. Leburton, and U. Ravaioli (Kluwer, Dordrecht, 1991), p. 259.
[24] M. Sumetskii, Phys. Rev. B **48**, 4586 (1993); **48**, 14 288 (1993); Appl. Phys. Lett. **63**, 3185 (1993); J. Phys. Condens. Matter **3**, 2651 (1991).
[25] C. S. Chu and R. S. Sorbello, Phys. Rev. B **40**, 5941 (1989); Z. Chen and R. S. Sorbello, *ibid.* **44**, 12 857 (1991).
[26] P. F. Bagwell, Phys. Rev. B **41**, 10 354 (1990); J. Phys. Condens. Matter **2**, 6179 (1990).
[27] E. Tekman and S. Ciraci, Phys. Rev. B **42**, 9098 (1990).
[28] Y. B. Levison, M. I. Lubin, and E. V. Sukhorukov, Phys. Rev. B **45**, 11 936 (1992).
[29] Y. Takagaki and D. K. Ferry, Phys. Rev. B **45**, 6715 (1992); **46**, 15 218 (1992).
[30] J. M. Mao, Y. Huang, and J. M. Zhou, J. Appl. Phys. **73**, 1853 (1993).
[31] S. A. Gurvitz and Y. B. Levinson, Phys. Rev. B **47**, 10 578 (1993).
[32] P. Exner and P. Seba, J. Math. Phys. **30**, 2574 (1989); Y. Avishai, D. Bessis, B. G. Giraud, and G. Mantica, Phys. Rev. B **44**, 8028 (1991).
[33] C. S. Lent, Appl. Phys. Lett. **56**, 2554 (1990).
[34] F. Sols and M. Macucci, Phys. Rev. B **41**, 11 887 (1990).
[35] A. Weisshaar, J. Lary, S. M. Goodnick, and V. K. Tripathi, Appl. Phys. Lett. **55**, 2114 (1989); J. Appl. Phys. **70**, 355 (1991); IEEE Electron Device Lett. **12**, 2 (1991).
[36] H. U. Baranger, Phys. Rev. B **42**, 11 479 (1990).
[37] R. L. Schult, D. G. Ravenhall, and H. W. Wyld, Phys. Rev. B **39**, 5476 (1988).

[38]C. S. Lent, Appl. Phys. Lett. **57**, 1678 (1990).
[39]K.-F. Berggren and Z.-L. Ji, Phys. Rev. B **43**, 4760 (1991).
[40]Y. Takagaki and D. K. Ferry, Phys. Rev. B **44**, 8399 (1991).
[41]M. Büttiker, Y. Imry, and M. Ya, Azbel, Phys. Rev. A **30**, 1982 (1984); M. Büttiker, Phys. Rev. B **32**, 1846 (1985).
[42]M. Cahay, S. Bandyopadhyay, and H. L. Grubin, Phys. Rev. B **39**, 12 989 (1989).
[43]D. Kowal, U. Sivan, O. Entin-Wohlman, and Y. Imry, Phys. Rev. B **42**, 9009 (1990).
[44]C. H. Wu and G. Mahler, Phys. Rev. B **43**, 5012 (1991).
[45]D. Y. K. Ko and J. C. Inkson, Phys. Rev. B **38**, 9945 (1988); Semicond. Sci. Technol. **3**, 791 (1988).
[46]T. B. Boykin, B. Pezeshki, and J. S. Harris, Jr., Phys. Rev. B **46**, 12 769 (1992).
[47]D. Z.-Y. Ting and T. C. McGill, Phys. Rev. B **47**, 7281 (1993).
[48]R. Wessel and M. Altarelli, Phys. Rev. B **39**, 12 802 (1989).
[49]C. Aversa and J. E. Sipe, Appl. Phys. Lett. **63**, 1975 (1993).
[50]E. Tekman and P. F. Bagwell, Phys. Rev. B **48**, 2553 (1993).
[51]U. Fano, Phys. Rev. **124**, 1866 (1961).
[52]J. Spector, H. L. Störmer, K. W. Baldwin, L. N. Pfeiffer, and K. W. West, Appl. Phys. Lett. **56**, 967 (1990); in *Nanostructures and Mesoscopic Systems* (Ref. 8), p. 107.
[53]S. Tarucha, Y. Hirayama, T. Saku, and Y. Horikoshi, in *Nanostructures and Mesoscopic Systems* (Ref. 8), p. 131.
[54]L. P. Kouwenhoven, F. W. J. Hekking, B. J. van Wees, C. J. P. M. Harmans, C. E. Timmering, and C. T. Foxon, Phys. Rev. Lett. **65**, 361 (1990).
[55]D. C. Miller, R. K. Lake, S. Datta, M. S. Lundstrom, M. R. Melloch, and R. Reifenberger, in *Nanostructure Physics and Fabrication* (Ref. 7), p. 165.
[56]K. Aihara, M. Yamamoto, and T. Mizutani, Jpn. J. Appl. Phys. **31**, L916 (1992).
[57]J. C. Wu, M. N. Wybourne, A. Weisshaar, and S. M. Goodnick, J. Appl. Phys. **74**, 4590 (1993).
[58]J. C. Wu, M. N. Wybourne, W. Yindeepol, A. Weisshaar, and S. M. Goodnick, Appl. Phys. Lett. **59**, 102 (1991); W. Yindeepol, A. Chin, A. Weisshaar, S. M. Goodnick, J. C. Wu, and M. N. Wybourne, in *Nanostructures and Mesoscopic Systems* (Ref. 8), p. 139.
[59]R. Behringer, G. Timp, H. U. Baranger, and J. E. Cunningham, Phys. Rev. Lett. **66**, 930 (1991).
[60]K. Ismail, S. Washburn, and K. Y. Lee, Appl. Phys. Lett. **59**, 1998 (1991).
[61]J. Liu, K. Ismail, K. Y. Lee, J. M. Hong, and S. Washburn, Phys. Rev. B **47**, 13 039 (1993).
[62]E. B. Becker, G. F. Carey, and J. T. Oden, *Finite Elements* (Prentice-Hall, Englewood Cliffs, NJ, 1981).
[63]P. J. Price, Phys. Rev. B **38**, 1994 (1988).
[64]M. Büttiker, IBM J. Res. Dev. **32**, 63 (1988).
[65]T. B. Bahder, C. A. Morrison, and J. D. Bruno, Appl. Phys. Lett. **51**, 1089 (1987); J. D. Bruno, T. B. Bahder, and C. A. Morrison, Phys. Rev. B **37**, 7098 (1988).
[66]G. García-Calderón, A. Rubio, and R. Romo, J. Appl. Phys. **69**, 3612 (1991); G. García-Calderón and A. Rubio, Phys. Rev. B **36**, 4462 (1987); G. García-Calderón, Solid State Commun. **62**, 441 (1987).
[67]G. Breit and E. Wigner, Phys. Rev. **49**, 519 (1936).
[68]G. Gamow, Z. Phys. **51**, 204 (1928).
[69]S. Datta, *Quantum Phenomena* (Addison-Wesley, Reading, MA, 1989).
[70]P. W. Anderson, D. J. Thouless, E. Abrahams, and D. S. Fisher, Phys. Rev. B **22**, 3519 (1980).
[71]D. S. Fisher and P. A. Lee, Phys. Rev. B **23**, 6851 (1981).
[72]It appears that only in pathological cases, when both phases "chase" each other, there is no transmission zero. In such cases, a zero and pole coincide and cancel each other. Minute changes in the geometry will cause the zero-pole pair to separate.
[73]J. E. Avron, A. Raveh, and B. Zur, Rev. Mod. Phys. **60**, 873 (1988).
[74]P. J. Price, Appl. Phys. Lett. **62**, 289 (1993).
[75]P. J. Price, Phys. Rev. B **48**, 17 301 (1993).
[76]W. Porod, Z. Shao, and C. S. Lent, Phys. Rev. B **48**, 8495 (1993).